ORIGINAL PAPER

3D-QSAR study of c-Src kinase inhibitors based on docking

Ran Cao · Na Mi · Huabei Zhang

Abstract Cancer is a significant world health problem for which efficient therapies are in urgent demand. c-Src has emerged as an attractive target for drug discovery efforts toward antitumor therapies. Toward this target several series of c-Src inhibitors that showed activity in the assay have been reported. In this article, 3D-QSAR models have been built with 156 anilinoquinazoline and quinolinecarbonitrile derivative inhibitors by using CoMFA and CoMSIA methods. These studies indicated that the QSAR models were statistically significant with high predictabilities (CoMFA model, q^2=0.590, r^2=0.855; CoMSIA model, q^2= 0.538, r^2=0.748). The details of c-Src kinase/inhibitor binding interactions in the crystal structure of complex provided new information for the design of new inhibitors. As a result, docking simulations were also conducted on the series of potent inhibitors. The flexible docking method, which was performed by the DOCK program, positioned all of the inhibitors into the active site to determine the probable binding conformation. The CoMFA and CoMSIA models based on the flexible docking conformations also yielded statistically significant and highly predictive QSAR models (CoMFA model, q^2=0.507, r^2=0.695; CoMSIA model, q^2= 0.463, r^2=0.734). Our models would offer help to better comprehend the structure-activity relationships that exist for this class of compounds and also facilitate the design of novel inhibitors with good chemical diversity.

Keywords CoMFA · CoMSIA · c-Src kinase inhibitor · Docking · 3D-QSAR

R. Cao · N. Mi · H. Zhang (✉)
Key Laboratory of radiopharmaceuticals of Ministry of Education,
College of Chemistry, Beijing Normal University,
Beijing 100875, China
e-mail: 496718650@qq.com

Introduction

c-Src kinase, a nonreceptor protein tyrosine kinase, plays critical role in a variety of cellular signal transduction pathways that are involved in cell division, motility, adhesion, angiogenesis, and survival [1]. c-Src kinase is expressed at low levels in most cell types and, in the absence of appropriate extracellular stimuli, maintains in an inactive conformation. In contrast to its highly regulated role in normal cells, emerging data [2] have shown that c-Src kinase is upregulated in many human tumor types [3, 4] and suggest that overexpression of it can be predictive of poor prognosis [5, 6]. Studies, mostly performed in colon cancer cells and fibroblasts [2], reveal that the oncogenic potential of increased Src activity in tumor cells [3, 4] is pleiotropic involving control of cell proliferation and the regulation of cytoskeletal-linked events [7], such as E-cadherin-mediated-adhesion [8, 9], migration [10], spreading [11], and invasion [12]. At the same time, more and more data suggest that c-Src kinase inhibition may enhance the anti-tumor efficacy of hormonal and cytotoxic agents in preclinical models. As shown by Duxbury *et al.* [13], c-Src inhibition may serve the dual function of increasing the sensitivity of pancreatic tumors to established chemotherapeutic agents and inhibiting the ability of these tumors to metastasize. In animal models, inhibition of Src expression and activity has been shown to inhibit tumor progression and metastasis of pancreatic tumor [14], and c-Src has represented an important candidate for targeted therapy in cancer [14–16]. Several c-Src kinase inhibitors have been identified to date including various scaffolds: dihyropyrimido-quinolinones [17], pyrazolo-pyrimidines [18], 4-anilinoquinazolines [19], and others [20, 21].

CoMFA [22] and CoMSIA [23] are two commonly used 3D-QSAR methodologies that have been employed to

recognize pharmacophoric units [24]. In CoMFA and CoMSIA studies, the conformation determination is so important that it affects the quality of a model. In most cases a bound complex is not available and therefore a computation method has to be deployed to determine conformations of a set of molecules [25]. In conventional ligand-based QSAR, it is through minimizing the molecules and selecting those with lowest energy that the active conformations are obtained. However, there is no guarantee that the conformation with the lowest energy is certainly the active conformation *in vivo*. As a result, the newly designed molecules based on such a model probably fail to bind the receptor even if the QSAR model is in good correlation with the experimental activity. While receptor-based conformation determination by docking takes into account features of the binding pocket, and thus derived models are more reliable. Several applications of docking with CoMFA have been reported [26, 27].

Previous 3D-QSAR study on the inhibitors of c-Src kinase has revealed some detailed and instructional information on the structural modifying at several substitutional positions such as the 3-position, aniline NH and 2'-, 5'-sites of aniline ring [21]. However, due to the limits of lacking accurate crystal structural information of the kinase-inhibitor complex, this model had not been tested and verified by the structural information of active method which has its own limits in aspects as mentioned above. Recently, a novel series of compounds as inhibitors of c-Src kinase have been synthesized which have the same backbone as the previous studied compounds but different substituent groups at 3-, 6-, 7-positions and additional substituent groups at 5-position. More importantly, the crystal structure [28] of Src kinase in complex with a quinazoline inhibitor has also been published, and thus it is necessary to build a 3D-QSAR model for these new compounds in a more effective way. In this study, we combined flexible docking with 3D-QSAR method to study these series of compounds and built our predicted model with good quality. Because the structural information of active site can be realized by the crystal structure of complex, in addition to docking alignment, the model is more creditable.

Materials and methods

Discarding inactive compounds and compounds with unspecified inhibitory activity, data from several separately published articles with the homogeneity of the biological assays were combined for our QSAR studies [21, 28, 29].

The total set of 156 compounds was randomly divided into a training set and test set comprisrd of 126 and 30 molecules respectively. To derive the CoMFA and CoMSIA

models, all the activity values of the c-Src inhibitors reported as IC_{50} in the literatures were converted to pIC_{50} (-$logIC_{50}$). Molecular structures and their pIC_{50} values were presented in Table 1.

The basic skeleton and conformation for providing a realistic pharmacophore was modeled after the structure of the ligand, which was extracted from the co-crystal complex 2H8H and changed atom types, added hydrogen by SYBYL7.0 program. Then the optimization of the structure using Tripos force field with Gasteiger-Huckel charges and minimization using conjugated gradient method till the root-mean-square deviation (RMSD) of 0.01 kcal mol^{-1} achieved were carried out. The obtained structure was used as the template to construct the 3D structures of all the other compounds. The side chains of all the compounds were subjected to a systematic search routine of rotatable bonds in 10° increments from 0° to 359° and rotatable rings in default parameters. Energies of conformations were computed and the lowest energy structures were used in alignment. The partial atomic charges required for electrostatic interaction were computed by semiempirical molecular orbital methods using MOPAC with AM1 Hamiltonian (key word: MMOK).

In 3D-QSAR studies, the common structure of a total of 156 compounds in our data derived from the same template molecule (compound AZD0530, Fig. 1) are highlighted with bold bonds in Table 1. This paper chose alignment of public skeleton (Fig. 2) firstly, and all the alignment was show in Fig. 3. They were performed with the Align Database of SYBYL 7.0.

All CoMFA and CoMSIA calculations were performed using SYBYL7.0. The charges were determined using the Gasteiger-Huckel method. The grid spacing was set at 2Å and the region was calculated automatically by the program. In CoMFA studies, a default sp^3-carbon atom having a charge of +1 and a van der Waals radius of 1.52 Å was used as a probe to generate steric (Lennard-Jones 6-12 potential) field and electrostatic (Coulombic potential) field energies with a distance-dependent dielectric at each lattice point. Both energy calculations were truncated to 30 kcal mol^{-1} for all grid points. CoMSIA technique was also applied in our studies in order to obtain more information to design novel selective drugs. The standard settings (sp^3-carbon probe atom with charge +1, VDW radius 1 Å, attenuation factor α of 0.3, grid spacing 2 Å) were used to calculate five different fields, viz. steric, electrostatic, hydrophobic, hydrogen acceptor and donor. Because of a Gaussian type distance dependence of the physicochemical properties, singularities were avoided at atomic positions and no arbitrary cutoffs were necessary.

PLS methodology is used to correlate c-Src inhibitor activities with the CoMFA and CoMSIA values. Column filtering value (σ) was set to 2.0 kcal mol^{-1} to improve the

Table 1 Structures and *in vitro* activities of compounds 1~156

No.	R1	R2	R3	X					pIC_{50}
				2'	3'	5'	6'		
1	(*N*-methylpiperidin 4-yl)oxy	H	H	Cl	H	CH_3O	H		6.52
2	Tetrahydropyran-4-yloxy	H	H	Cl	H	CH_3O	H		6.4
3[a]	(*N*-methylpiperidin-4-yl)oxy	H	H	OCH_2O		H	Cl		7
4	(*N*-methylpiperidin-4-yl)oxy	H	CH_3O	Cl	H	CH_3O	H		6.64
5	(*N*-methylpiperidin-4-yl)oxy	H	CH_3O	Cl	H	CH_3O	H		7.52
6	(*N*-methylpiperidin-4yl)oxy	H	CH_3O	OCH_2O		H	Cl		8
7	Tetrahydropyran-4-yloxy	H	Morpholinyl -$(CH_2)_3O$	Cl	H	CH_3O	H		7.7
8[a]	cyclohexyloxy	H	Morpholinyl -$(CH_2)_3O$	Cl	H	CH_3O	H		7.7
9	isopropoxy	H	Morpholinyl -$(CH_2)_3O$	Cl	H	CH_3O	H		7.4
10	Tetrahydropyran-4-yloxy	H	Pyrrolidinyl -$(CH_2)_3O$	OCH_2O		H	H		7.4
11	(*N*-methylpiperidin-4-yl)oxy	H	CH_3O	OCH_2O		H	H		6.82
12[a]	(*N*-methylpiperidin-4-yl)oxy	H	CH_3O	OCH_2CH_2O		H	H		6.24
13	Tetrahydropyran-4-yloxy	H	pyrrolidinyl- $(CH_2)_2O$	OCH_2O		H	H		7.1
14	Tetrahydropyran-4-yloxy	H	pyrrolidinyl- $(CH_2)_2O$	OCH_2O		H	Cl		8.4
15	Tetrahydropyran-4-yloxy	H	pyrrolidinyl- $(CH_2)_2O$	OCH_2O		H	Cl		8.22
16	Tetrahydropyran-4-yloxy	H	pyrrolidinyl-$(CH_2)_2O$	OCH_2CH_2O		H	H		7.07
17[a]	Tetrahydropyran-4-yloxy	H	(*N*-methylpiperidin-4-yl)methoxy	OCH_2O		H	Cl		8.22
18	Tetrahydropyran-4-yloxy	H	(pyridin-4-yloxy)ethoxy	OCH_2O		H	Cl		8.52
19	morpholinyl	H	pyrrolidinyl-$(CH_2)_2O$	OCH_2O		H	Cl		7.12
20	Tetrahydropyran-4-yloxy	H	(*N*-methylpiperazin-4-yl) propoxy	Cl	H	H	H		8.4
21	H	CH_3O	CH_3O	Cl	H	CH_3O	H		6.6
22[a]	piperidin-4-yloxy	H	H	OCH_2O		H	H		7.26
23	piperidin-4-yloxy	H	CH_3O	OCH_2O		H	Cl		8.02
24	Tetrahydropyran-4-yloxy	H	(*N*-methylpiperazin-4-yl) propoxy	OCH_2O		H	Cl		8.4

Table 1 (continued)

No.	R1	R2	R3	X				pIC$_{50}$
				2'	3'	5'	6'	
25	(*N*-methylpiperidin-4-yl)methoxy	H	H	OCH_2O		H	Cl	6.3
26	(*N*-methylpiperidin-4-yl)oxy	H	isopropoxy	OCH_2O		H	Cl	7
27[a]	(*N*-methylpiperidin-4-yl)oxy	H	2-fluoroethoxy	OCH_2O		H	Cl	8.4
28	(*N*-methylpiperidin-4-yl)oxy	H	isobutoxy	OCH_2O		H	Cl	8.15
29	isopropoxy	H	pyrrolidinyl-$(CH_2)_3O$	OCH_2O		H	Cl	8.4
30	isopropoxy	H	Morpholinyl -$(CH_2)_2O$	OCH_2O		H	Cl	8.3
31	isopropoxy	H	(acetylpiperazinyl) ethoxy	OCH_2O		H	F	7.7
32[a]	Tetrahydropyran -4-yloxy	H	(*N*-methylpiperazin -4-yl)ethoxy	OCH_2O		H	Cl	8.57
33	H	CH_3O	(*N*-methylpiperidin -4-yl)methoxy	OCH_2O		CH_3O	Cl	8.3
34	H	CH_3O	(*N*-methylpiperidin -4-yl)methoxy	Cl	H	H	H	8
35	CH_3O	H	pyrrolidinyl-$(CH_2)_3O$	OCH_2O		H	Cl	7.82
36	H	CH_3O	pyrrolidinyl-$(CH_2)_3O$	OCH_2O		H	Cl	8.3
37[a]	(*N*-methylpiperidin-4-yl)oxy	CH_3O	H	Cl	H	CH_3O	H	6.27
38	CH3O	H	CH_3O	Cl	H	CH_3O	H	5.43
39	Tetrahydropyran-4-yloxy	(*N*-methylpiperazin-4-yl)propoxy	H	Cl	H	CH_3O	H	6.22
40	Tetrahydropyran-4-yloxy	H	(*N*-methylpiperazin-4-yl)propoxy	OCH_2CH_2O	H	Cl		6.69
41	Tetrahydropyran-4-yloxy	H	(*N*-methylpiperazin-4-yl)ethoxy	OCH_2CH_2O	H	Cl		7.19
42[a]	H	MeO	MeO	H	MeO	H	H	6.6
43	H	MeO	4-morpholinyl -$(CH_2)_3O$	H	MeO	H	H	7.43
44	H	MeO	4-morpholinyl -$(CH_2)_3O$	MeO	H	H	H	6.25
45	H	MeO	4-morpholinyl -$(CH_2)_3O$	H	H	MeO	H	6.32
46	H	MeO	4-morpholinyl -$(CH_2)_3O$	H	EtO	H	H	8
47[a]	H	MeO	4-N-methyl poperidinyl-CH_2O	H	MeO	H	H	6.01
48	H	MeO	4-morpholinyl-$(CH_2)O$	2'-CHCHO-3'	H	H		7.8
49	H	MeO	4-morpholinyl-$(CH_2)_3O$	2'-CHCHO-3'	Cl	H		8
50	H	MeO	4-morpholinyl-$(CH_2)_3O$	2'-OCHCH-3'	H	H		7.52
51	H	MeO	4-morpholinyl-$(CH_2)_3O$	2'-OCHCH-3'	H	Cl		8
52[a]	H	MeO	4-morpholinyl-$(CH_2)_3O$	2'-OCH_2CH_2-3'	H	H		6.36
53	H	MeO	4-morpholinyl-$(CH_2)_3O$	2'-OCHCClH-3'	H	H		8.4
54	H	MeO	4-morpholinyl-$(CH_2)_3O$	2'-CHCHNH-3'	H	H		6.75
55	H	MeO	4-morpholinyl-$(CH_2)_3O$	2'-CHCHNCH$_3$-3'	H	H		7.4
56	H	MeO	4-morpholinyl-$(CH_2)_3O$	2'-NHCHCH-3'	H	H		6.59
57[a]	H	MeO	4-morpholinyl-$(CH_2)_3O$	2'-NHCHCCl-3'	H	H		7.7

Generic structure for both tables.

Compounds 58–69

No.	R1	R2	R3	X	Y	pIC$_{50}$
58	MeO	4-morpholinyl-$(CH_2)_3$O	OCH_2O	H	H	7.85
59	MeO	4-morpholinyl-$(CH_2)_3$O	OCH_2O	Cl	H	8.4
60	MeO	4-morpholinyl-$(CH_2)_3$O	OCH_2O	Br	H	8.4
61	MeO	4-morpholinyl-$(CH_2)_3$O	OCH_2O	F	H	7.55
62[a]	MeO	4-morpholinyl-$(CH_2)_3$O	OCF_2O		H	6.57
63	MeO	4-morpholinyl-$(CH_2)_3$O	H		H	6.12
64	MeO	4-morpholinyl -$(CH_2)_3$O	OCH_2CH_2O	H	Cl	6.43
65	MeO	4-morpholinyl -$(CH_2)_3$O	OCH_2O	H	Cl	8
66[a]	4-morpholinyl-$(CH_2)_3$O	MeO	OCH_2O	H	Cl	7.3
67[a]	MeO	(N-methylpiperidin-4-yl)-(CH_2)OO	OCH_2O	H	Cl	8.3
68	MeO	Piperidinyl-$(CH_2)_2$OO	OCH_2O	H	Cl	8.4
69	MeO	(2-cyanopyridin-4-yl)CH_2OO	OCH_2O	H	Cl	8

Compounds 70–85
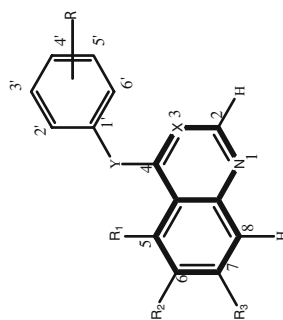
No.	R	R1	R2	R3	X	Y	pIC$_{50}$
70	3,4,5-trimethoxy	H	OMe	OMe	N	NH	6.55
71	3,5-dimethoxy-4-ethoxy	H	OMe	OMe	N	NH	6.47
72[a]	3,5-dimethoxy-4-n-butoxy	H	OMe	OMe	N	NH	6.31
73	3,5-dimethoxy-4-t-butoxy	H	OMe	OMe	N	NH	6.08
74	3,5-dimethoxy-4-isopropoxy	H	OMe	OMe	N	NH	5.57
75	3,4,5-trimethoxy	H	OMe	OMe	C-CN	NH	7.46
76	3,5-dimethoxy-4-ethoxy	H	OMe	OMe	C-CN	NH	7.20
77[a]	3,5-dimethoxy-4-isopropoxy	H	OMe	OMe	C-CN	NH	6.96
78	3,4-dimethoxy	H	OMe	OMe	C-CN	NH	6.02
79	2-Bromo-3,4,5-trimethoxy	H	OMe	OMe	C-CN	NH	6.77
80	3,4,5-trimethoxy	H	OMe	OMe	CH	NH	6.70
81	3,4,5-trimethoxy	H	OMe	OMe	C-CN	O	6.54
82[a]	2,4-diCl	H	OMe	OMe	C-CN	NH	7.52
83	2,4-diCl	H	OMe	OMe	N	NH	6.60
84	2,4-diCl	H	OMe	OMe	CH	NH	7.08
85	2,4-diCl	H	OMe	OMe	C-CN	S	5.66

Table 1 (continued)

No.	R1	R2	R3	X				pIC$_{50}$
				2'	3'	5'	6'	
86	2,4-diCl	OMe	OMe		H	C-CHO	NH	6.60
87[a]	2,4-diCl	H	H		OMe	C-CN	NH	5.92
88	2,4-diCl	H	OMe		H	C-CN	NH	6.49
89	2,4-diCl	OMe	H		H	C-CN	NH	6.70
90	2,4-diCl	OEt	OEt		H	C-CN	NH	7.96
91	2,4-diCl	O-n-Bu	O-n-Bu		H	C-CN	NH	6.80
92[a]	2-Cl	OMe	OMe		H	C-CN	NH	7.02
93	4-Cl	OMe	OMe		H	C-CN	NH	7.28
94	2,3-diCl	OMe	OMe		H	C-CN	NH	7.05
95	2,5-diCl	OMe	OMe		H	C-CN	NH	7.40
96	2,6-diCl	OMe	OMe		H	C-CN	NH	7.21
97[a]	3,5-diCl	OMe	OMe		H	C-CN	NH	5.96
98	3,4-diCl	OMe	OMe		H	C-CN	NH	7.24
99	2-F,4-Cl	OMe	OMe		H	C-CN	NH	7.28
100	2-Br,4-Cl	OMe	OMe		H	C-CN	NH	8.00
101	2-I,4-Cl	OMe	OMe		H	C-CN	NH	8.21
102[a]	2-Cl,4-I	OMe	OMe		H	C-CN	NH	7.02
103	2-Cl,4-Br	OMe	OMe		H	C-CN	NH	7.82
104	2,4-diCl	(CH$_2$)$_3$-morpholine	(CH$_2$)$_3$-morpholine		H	C-CN	NH	7.72
105	2,4-diCl	Me	(CH$_2$)$_3$-morpholine		H	C-CN	NH	6.66
106	2,4-diCl	(CH$_2$)$_3$-morpholine	Me		H	C-CN	NH	8.42
107[a]	2,4-diCl	(CH$_2$)$_3$-N-methyl-piperazine	Me		H	C-CN	NH	8.06
108	2,4-diCl	(CH$_2$)$_3$-4-nydroxy-piperidine	Me		H	C-CN	NH	8.46
109	2-Cl,5-OMe	OMe	OMe		H	C-CN	NH	8.00
110	2,4-di-Cl,5-OMe	OMe	OMe		H	C-CN	NH	8.37
111	2,4-di-Cl,5-OEt	OMe	OMe		H	C-CN	NH	5.92
112[a]	2,4-di-Cl,5-OH	OMe	OMe		H	C-CN	NH	6.72
113	2-F,4-Cl,5-OMe	OMe	OMe		H	C-CN	NH	7.18
114	2-Br,4-Cl,5-OMe	OMe	OMe		H	C-CN	NH	8.52
115	2-Me,4-Cl,5-OMe	OMe	OMe		H	C-CN	NH	8.40
116	4-Cl,3-OMe	OMe	OMe		H	C-CN	NH	6.92
117[a]	2-Cl,4-Me,5-OMe	OMe	OMe		H	C-CN	NH	8.54
118	2,4-di-Me,5-OMe	OMe	OMe		H	C-CN	NH	8.34

No.							
119	2,4-di-Me,5-OMe	OMe	OMe	H	N	NH	6.41
120	2,4-di-Cl,5-OMe	OMe	OMe	H	CH	NH	7.09
121	2-Cl,5-OMe	O-(CH2)3-morpholine	OMe	H	C-CN	NH	8.80
122[a]	2,4-di-Cl,5-OMe	O-(CH2)3-morpholine	OMe	H	C-CN	NH	9.10
123	2-Br,4-Cl,5-OMe	O-(CH2)3-morpholine	OMe	H	C-CN	NH	9.02
124	2-Me,4-Cl,5-OMe	O-(CH2)3-morpholine	OMe	H	C-CN	NH	8.92
125	2,4-di-Me,5-OMe	O-(CH2)3-morpholine	OMe	H	C-CN	NH	8.77
126	2-Cl,4-Me,5-OMe	O-(CH2)3-morpholine	OMe	H	C-CN	NH	8.96
127[a]	2,4-di-Cl,5-OMe	O-(CH2)4-morpholine	OMe	H	C-CN	NH	8.89
128	2,4-di-Cl,5-OMe	O-(CH2)5-morpholine	OMe	H	C-CN	NH	8.60
129	2,4-di-Cl,5-OMe	O-(CH2)3-N-Methylpiperazine	OMe	H	C-CN	NH	8.92
130	2,4-di-Cl,5-OMe	O-(CH2)3-N-ethylpiperazine	OMe	H	C-CN	NH	9.11
131	2,4-di-Cl,5-OMe	O-(CH2)3-cis-3,4,5-tri-Me-Piperazine	OMe	H	C-CN	NH	8.85
132[a]	2,4-di-Cl,5-OMe	O-(CH2)3-4-n-Pr-piperazine	OMe	H	C-CN	NH	8.96
133	2,4-di-Cl,5-OMe	O-(CH2)3-piperazine	OMe	H	C-CN	NH	8.96
134	2,4-di-Cl,5-OMe	O-(CH2)3-4-(CH2)2OH-piperazine	OMe	H	C-CN	NH	9.12
135	2,4-di-Cl,5-OMe	O-(CH2)3-4-Me-homopiperazine	OMe	H	C-CN	NH	8.85
136	2,4-di-Cl,5-OMe	O-(CH2)3-piperidine	OMe	H	C-CN	NH	8.92
137[a]	2,4-di-Cl,5-OMe	O-(CH2)3-4-OH-piperidine	OMe	H	C-CN	NH	9.19
138	2,4-di-Cl,5-OMe	O-(CH2)3-2-(1,2,3-triazole)	OMe	H	C-CN	NH	8.03
139	2,4-di-Cl,5-OMe	O-(CH2)3-1-(1,2,3-triazole)	OMe	H	C-CN	NH	8.72
140	2,4-di-Cl,5-OMe	O-(CH2)3-1-imidazole	OMe	H	C-CN	NH	8.63
141	2,4-di-Cl,5-OMe	O-(CH2)3-NH(CH2)2-morpholine	OMe	H	C-CN	NH	8.52
142[a]	2,4-di-Cl,5-OMe	O-(CH2)3-NMe(CH2)2NMe	OMe	H	C-CN	NH	8.64
143	2,4-di-Cl,5-OMe	O-(CH2)3-(N-methylpiperidin-4-yl)	OMe	H	C-CN	NH	8.42
144	2,4-di-Cl,5-OMe	O-(CH2)- (N-methylpiperidin-4-yl)	OMe	H	C-CN	NH	8.15
145	2,4-di-Cl,5-OMe	O-(CH2)2-(N-methylpiperidin-4-yl)	OMe	H	C-CN	NH	8.11
146	2,4-di-Cl,5-OMe	O-(CH2)3-Me-piperazine	OMe	H	C-CN	NH	8.57
147[a]	2,4-di-Cl,5-OMe	O-(N-methylpiperidin-4-yl)	OMe	H	C-CN	NH	6.64
148	2,4-di-Cl,5-OMe	2-sub analog of 145	OMe	H	C-CN	NH	7.06
149	2,4-di-Cl,5-OMe	3-sub analog of 145	OMe	H	C-CN	NH	8.05
150	2,4-di-Cl	O-(CH2)- (N-methylpiperidin-4-yl)	OMe	H	C-CN	NH	7.68
151	3,4,5-trimethoxy	O-(CH2)- (N-methylpiperidin-4-yl)	OMe	H	C-CN	NH	7.46
152	2-Cl,5-OMe	O-(CH2)- (N-methylpiperidin-4-yl)	OMe	H	C-CN	NH	7.92
153	2-Me,5-OMe	O-(CH2)- (N-methylpiperidin-4-yl)	OMe	H	C-CN	NH	7.62
154	2,4-di-Me	O-(CH2)- (N-methylpiperidin-4-yl)	OMe	H	C-CN	NH	7.20
155	2,4-di-Me,5-OMe	O-(CH2)- (N-methylpiperidin-4-yl)	OMe	H	C-CN	NH	7.89
156	2,4-di-Cl,5-OEt	O-(CH2)-(N-methylpiperidin-4-yl)	OMe	H	C-CN	NH	5.85

[a] molecules belonged to the test set

Fig. 1 Compound AZD0530

Fig. 3 Alignment of 156 inhibitors using Align Database
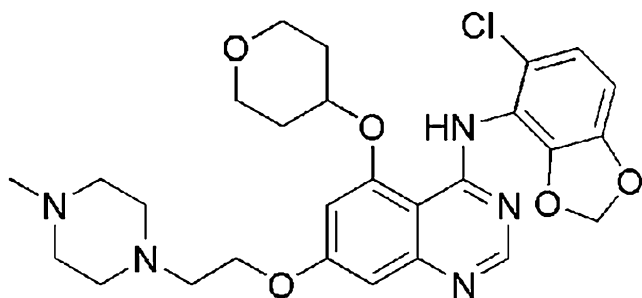
signal-to-noise ratio. The predictive value of the models was evaluated first by leave-one-out (LOO) cross-validation. The cross-validated coefficient q^2 was calculated according to the following equation:

$$q^2 = 1 - \frac{\sum \left(Y_{pred} - Y_{actu}\right)^2}{\sum \left(Y_{actu} - Y_{mean}\right)^2}$$

Where Y_{pred}, Y_{actu} and Y_{mean} are predicted, actual and mean values of the target property (pIC_{50}), respectively; and

$$\sum \left(Y_{actu} - Y_{mean}\right)^2 = PRESS$$

PRESS is the prediction error sum of the squares, derived from the LOO method. The optimum number of components (ONC) corresponding to the lowest PRESS value was used for deriving the final PLS regression models. In addition to the q^2 and ONC, the conventional correlation coefficient (r^2), standard error of estimate (SE) and F-ratio (F) were also computed.

The docking studies of the database composed of all 156 compounds were performed with the DOCK6.0 software [30, 31] which allows scientists to explore high-throughput molecular docking. Hydrogen and partial charges based on Amber99 were assigned on the protein receptor using the Chimera program. The molecule surface data were created with the DMS program for the sphere calculation. Spheres were generated with the SPHGEN program [32]. The relevant spheres which were 10.0 Å out from the coordinates of the ligand from the crystal structure were selected for the grid and docking computations. The box for

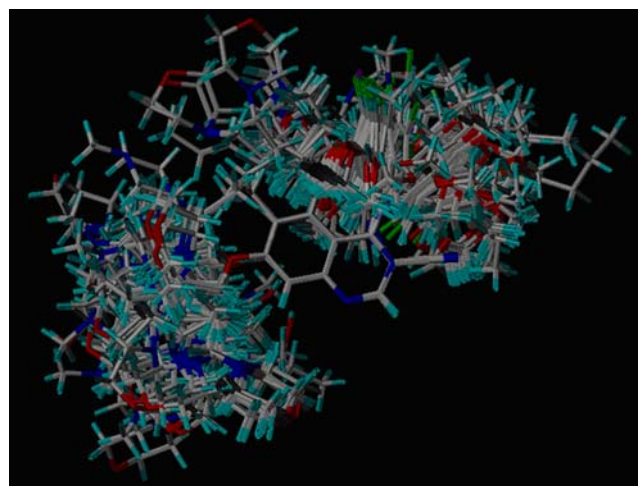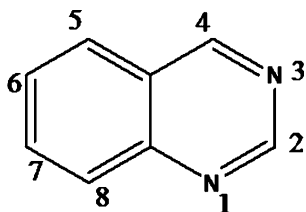scoring grid was defined that all spheres were enclosed with 5.0 added in each dimension. Scoring grids for energy scores were calculated with a grid spacing of 0.3 Å. Ligand atoms were matched to receptor spheres using the anchor first search with the anchor size set to 40 atoms. All of the inhibitors were docked allowing for ligand's flexibility using the grid based energy scoring option for minimization after initial placement in the site. The maximum of orientation was set to 500 for the anchor fragment.

In this study, all molecules were aligned according to the bound position in the active binding pocket of c-Src kinase using flexible docking. In docking alignment each molecule tried to fit the binding pocket of c-Src kinase in terms of steric and electronic interactions with the enzyme. The poses of these inhibitors had similar binding positions and the same orientation with each other and with the AZD0530 in the crystal complex. Therefore, the resulting model encoded the feature of the binding site and would be more reasonable for the study of activity than the ligand-based model.

Results and discussion

CoMFA analysis of c-Src was performed based on the conformational alignment of 126 compounds. The remaining 30 compounds were put into the test set for model validation. PLS analysis of c-Src inhibitors of training set showed cross-validated q^2 of 0.590 using five principal components and non-cross-validated r^2 value of 0.855. The results of CoMFA analysis are summarized in Table 2. These values indicated a good statistical correlation and internal predictability of CoMFA model. The correlation between the actual and the predicted values from the final CoMFA model are shown in Fig. 4a.

Fig. 2 Public skeleton

Table 2 Statistical parameters of CoMFA and CoMSIA models of the training sets

	ONC	PRESS	q^2	r^2	SE	F	Field contribution				
							steric	electrostatic	hydrophobic	donor	acceptor
CoMFA	5	0.617	0.590	0.855	0.367	141.039	0.518	0.482			
CoMSIA	4	0.660	0.538	0.748	0.482	89.625	0.189	0.267	0.282	0.107	0.155

The CoMSIA method defines explicit hydrophobic, hydrogen bond donor and acceptor descriptors in addition to steric and electrostatic fields used in CoMFA. Using default CoMSIA parameters, all compounds in the c-Src

Fig. 4 Correlation between the actual and predicted activities of 3D QSAR models for the training set and test set. (**a** CoMFA model; **b** CoMSIA model. ▲: compounds of the training set; ▽: compounds of the test set)

inhibitors training set and all five descriptors, we derived a model with high q^2 value of 0.538 for four components and a conventional r^2 value of 0.748. CoMSIA analysis results are also summarized in Table 2. These data indicated that a reliable CoMSIA model was successfully constructed. Predicted activities by this model versus experimental activities of inhibitors are displayed in Fig. 4b. It can be seen clearly from Fig. 4 that the predicted pIC_{50} values obtained from CoMFA and CoMSIA models are in good agreement with the actual data. The predicted activities of all 156 compounds for both CoMFA and CoMSIA models were also listed in Table 3.

Before docking the derivatives of the total set into the c-Src allosteric binding site with DOCK6.0 package, the docking protocol was validated. The AZD0530 (a quinazoline inhibitor) extracted from the crystal structure of complex (Protein Data Bank, http://www.rcsb.org/pdb/, PDB ID code 2H8H) was docked back into the active binding groove of c-Src kinase. The root mean squares deviation (RMSD) between the predicted conformation and the observed X-ray crystallographic conformation of compound AZD0530 was 1.34 Å. Thus molecular docking produced a good solution when compared to the existing X-ray structure and suggested that an overall inhibitor alignment could be used in 3D-QSAR analyses.

The CoMFA and CoMSIA studies based on the flexible docking alignment were also conducted. The docked conformation for each molecule was chosen on the basis of the grid score which is based on an estimation of van der Waal attractive, van der Waal dispersive and Coulombic electrostatic energies. The results of CoMFA and CoMSIA analysis of the training set are summarized in Table 4 and the predicted versus experimental activities are displayed in Fig. 5a and b. The comparison of the predictive index of QSAR models based on both align database and flexible docking alignment methods for the test set is shown in Table 5.

The models generated from flexible docking alignment showed a lower statistics than those based on the align database method. However, in conventional ligand-based QSAR, it is through minimizing the molecules and selecting those with lowest energy that the active con-
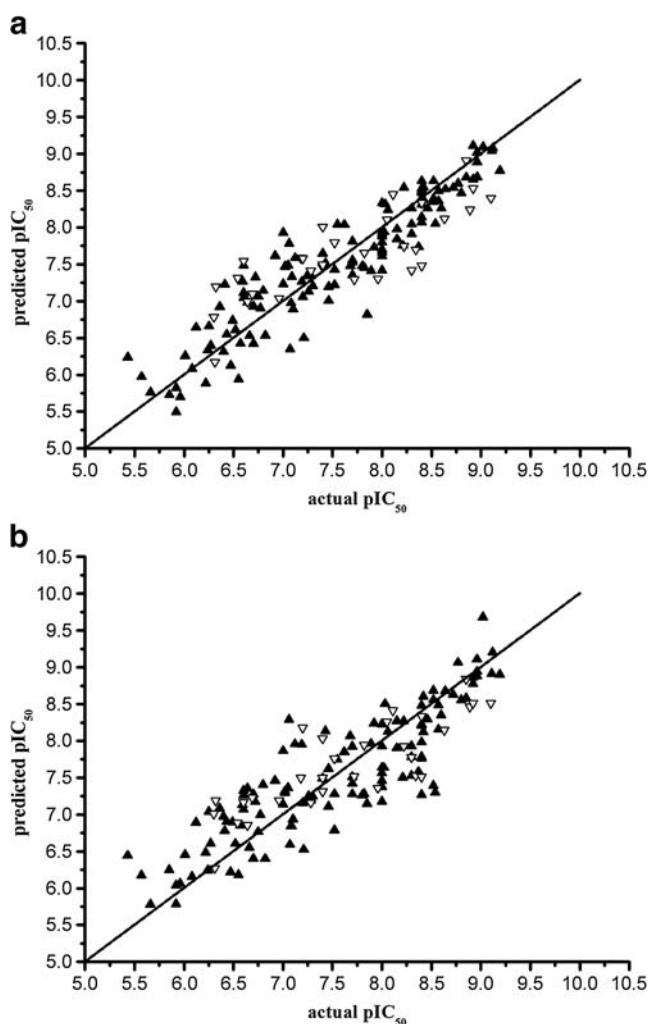
Table 3 Comparison of actual and predicted pIC_{50} values of all 156 compounds for CoMFA and CoMSIA models

No.	pIC_{50}	fa-pre[a]	fa-D[b]	sia-pre[c]	sia-D[d]	No.	pIC_{50}	fa-pre	fa-D	sia-pre	sia-D
1	6.55	5.943	0.607	6.181	0.369	79	8.64	8.522	0.118	8.68	-0.04
2	6.47	6.128	0.342	6.221	0.249	80	8.42	8.551	-0.131	8.607	-0.187
3[e]	6.31	6.173	0.137	6.271	0.039	81	8.15	7.843	0.307	8.274	-0.124
4	6.08	6.086	-0.006	6.16	-0.08	82[e]	8.11	8.452	-0.342	8.413	-0.303
5	5.57	5.977	-0.407	6.175	-0.605	83	8.57	8.498	0.072	8.489	0.081
6	7.46	7.009	0.451	7.112	0.348	84	6.64	6.985	-0.345	7.356	-0.716
7	7.2	7.059	0.141	7.159	0.041	85	7.06	7.784	-0.724	8.292	-1.232
8[e]	6.96	7.038	-0.078	7.193	-0.233	86	7.7	7.531	0.169	7.422	0.278
9	6.52	6.608	-0.088	6.607	-0.087	87[e]	8.05	8.104	-0.054	8.258	-0.208
10	6.77	6.905	-0.135	6.999	-0.229	88	7.68	7.48	0.2	8.07	-0.39
11	6.7	6.424	0.276	6.402	0.298	89	7.46	7.196	0.264	7.623	-0.163
12[e]	6.54	7.312	-0.772	6.887	-0.347	90	7.92	7.732	0.188	8.241	-0.321
13	7.52	7.429	0.091	7.279	0.241	91	7.62	8.04	-0.42	7.852	-0.232
14	6.6	7.117	-0.517	7.074	-0.474	92[e]	7.2	7.578	-0.378	8.178	-0.978
15	7.08	6.978	0.102	6.845	0.235	93	7.89	7.412	0.478	7.966	-0.076
16	5.66	5.763	-0.103	5.781	-0.121	94	5.85	5.729	0.121	6.25	-0.4
17[e]	6.6	7.545	-0.945	7.166	-0.566	95	8.4	8.315	0.085	7.785	0.615
18	5.92	5.499	0.421	6.041	-0.121	96	7.4	7.649	-0.249	7.492	-0.092
19	6.49	6.739	-0.249	6.9	-0.41	97[e]	7.4	7.491	-0.091	7.498	-0.098
20	6.4	6.316	0.084	6.975	-0.575	98	6.82	6.535	0.285	6.403	0.417
21	6.7	6.931	-0.231	7.278	-0.578	99	6.24	6.336	-0.096	6.244	-0.004
22[e]	7.96	7.304	0.656	7.36	0.6	100	7.1	6.892	0.208	6.939	0.161
23	6.8	7.144	-0.344	7.405	-0.605	101	8.4	8.498	-0.098	8.227	0.173
24	7.02	7.466	-0.446	7.293	-0.273	102[e]	8.22	7.747	0.473	7.929	0.291
25	7.28	7.344	-0.064	7.197	0.083	103	7.07	6.349	0.721	6.594	0.476
26	7.05	7.487	-0.437	7.363	-0.313	104	8.22	8.546	-0.326	8.274	-0.054
27[e]	7.4	7.46	-0.06	7.314	0.086	105	8.52	8.353	0.167	8.56	-0.04
28	7.21	6.501	0.709	6.526	0.684	106	7.12	7.589	-0.469	7.959	-0.839
29	5.96	5.7	0.26	6.064	-0.104	107[e]	8.4	7.479	0.921	7.511	0.889
30	7.24	7.342	-0.102	7.212	0.028	108	6.6	7.486	-0.886	7.328	-0.728
31	7	7.234	-0.234	7.142	-0.142	109	7.26	7.136	0.124	7.252	0.008
32[e]	7.28	7.411	-0.131	7.163	0.117	110	8.02	7.94	0.08	7.638	0.382
33	8	7.421	0.579	7.378	0.622	111	8.4	8.532	-0.132	8.483	-0.083
34	8.21	7.755	0.455	7.506	0.704	112[e]	6.3	6.785	-0.485	7.01	-0.71
35	7.02	7.476	-0.456	7.317	-0.297	113	7	7.933	-0.933	7.866	-0.866
36	7.82	7.457	0.363	7.282	0.538	114	8.4	8.475	-0.075	7.764	0.636
37[e]	7.72	7.294	0.426	7.516	0.204	115	8.15	7.98	0.17	7.905	0.245
38	6.66	6.532	0.128	6.555	0.105	116	8.4	8.143	0.257	7.984	0.416
39	8.42	8.381	0.039	8.123	0.297	117[e]	8.3	7.418	0.882	7.775	0.525
40	8.06	8.242	-0.182	8.128	-0.068	118	7.7	7.816	-0.116	7.925	-0.225
41	8.46	8.263	0.197	8.295	0.165	119	8.57	8.363	0.207	8.159	0.411
42[e]	6.64	6.994	-0.354	6.856	-0.216	120	8.3	8.264	0.036	7.53	0.77
43	8	7.703	0.297	7.564	0.436	121	8	7.947	0.053	7.374	0.626
44	8.37	7.738	0.632	7.583	0.787	122[e]	7.82	7.657	0.163	7.943	-0.123
45	5.92	5.826	0.094	5.787	0.133	123	8.3	7.915	0.385	7.782	0.518
46	6.72	7.328	-0.608	7.175	-0.455	124	6.27	6.401	-0.131	6.608	-0.338
47[e]	7.18	7.586	-0.406	7.499	-0.319	125	5.43	6.237	-0.807	6.445	-1.015
48	8.52	8.395	0.125	7.394	1.126	126	6.22	5.886	0.334	6.487	-0.267
49	8.4	8.482	-0.082	7.272	1.128	127[e]	6.69	7.099	-0.409	7.231	-0.541

Table 3 (continued)

No.	pIC$_{50}$	fa-pre[a]	fa-D[b]	sia-pre[c]	sia-D[d]	No.	pIC$_{50}$	fa-pre	fa-D	sia-pre	sia-D
50	6.92	7.618	-0.698	7.464	-0.544	128	7.19	7.267	-0.077	7.955	-0.765
51	8.54	8.052	0.488	7.302	1.238	129	6.6	7.046	-0.446	7.265	-0.665
52[e]	8.34	7.7	0.64	7.527	0.813	130	7.43	7.519	-0.089	8.136	-0.706
53	7.52	7.222	0.298	6.79	0.73	131	6.25	6.662	-0.412	7.043	-0.793
54	6.41	7.226	-0.816	6.779	-0.369	132[e]	6.32	7.197	-0.877	7.189	-0.869
55	7.09	7.332	-0.242	6.841	0.249	133	8	7.616	0.384	7.638	0.362
56	8.8	8.471	0.329	8.557	0.243	134	6.01	6.256	-0.246	6.455	-0.445
57[e]	9.1	8.399	0.701	8.513	0.587	135	7.8	7.477	0.323	7.263	0.537
58	9.02	9.095	-0.075	9.681	-0.661	136	8	7.666	0.334	7.179	0.821
59	8.92	9.114	-0.194	8.864	0.056	137[e]	7.52	7.797	-0.277	7.762	-0.242
60	8.77	8.598	0.172	9.066	-0.296	138	8	8.335	-0.335	8.23	-0.23
61	8.96	9.02	-0.06	9.11	-0.15	139	6.36	6.924	-0.564	7.085	-0.725
62[e]	8.89	8.241	0.649	8.465	0.425	140	8.4	8.073	0.327	7.761	0.639
63	8.6	8.262	0.338	8.354	0.246	141	6.75	7.063	-0.313	6.767	-0.017
64	8	7.799	0.201	7.38	0.62	142[e]	7.4	8.01	-0.61	8.033	-0.633
65	8.92	8.655	0.265	8.779	0.141	143	6.59	7.268	-0.678	7.132	-0.542
66	9.11	9.044	0.066	8.914	0.196	144	7.7	7.357	0.343	7.281	0.419
67[e]	8.85	8.912	-0.062	8.839	0.011	145	7.85	6.82	1.03	7.146	0.704
68	8.96	8.892	0.068	8.882	0.078	146	8.4	8.401	-1E-3	8.221	0.179
69	8.96	8.685	0.275	8.943	0.017	147[e]	8.4	8.335	0.065	8.337	0.063
70	9.12	9.078	0.042	9.205	-0.085	148	7.55	8.042	-0.492	7.749	-0.199
71	8.85	8.684	0.166	8.581	0.269	149	6.57	6.426	0.144	6.854	-0.284
72[e]	8.92	8.53	0.39	8.514	0.406	150	6.12	6.644	-0.524	6.895	-0.775
73	9.19	8.771	0.419	8.904	0.286	151	6.43	6.552	-0.122	6.908	-0.478
74	8.03	8.319	-0.289	8.503	-0.473	152	8	7.881	0.119	7.93	0.07
75	7.7	7.557	0.143	7.513	0.187	153	7.3	7.209	0.091	7.249	0.051
76	8.72	8.542	0.178	8.63	0.09	154	8.3	8.046	0.254	7.931	0.369
77[e]	8.63	8.12	0.51	8.149	0.481	155	8.4	8.633	-0.233	8.209	0.191
78	8.52	8.634	-0.114	8.687	-0.167	156	8	7.91	0.09	7.463	0.537

[e]: molecules belonged to the test set; a: predicted pIC$_{50}$ values for CoMFA model; b: residues between actual and predicted pIC$_{50}$ values for CoMFA model; c: predicted pIC$_{50}$ values for CoMSIA model; d: residues between actual and predicted pIC$_{50}$ values for CoMSIA model

formations are obtained. There is no guarantee that the conformation with the lowest energy is certainly the active conformation *in vivo*. As a result, the newly designed molecules based on such a model probably fail to bind the receptor even if the QSAR model is in good correlation with the experimental activity. While structure-based conformation determination by flexible docking takes into account features of the binding pocket, and thus derived models are more reliable. So the docking-based QSAR study has the advantages over ligand-based QSAR allowing for many more differences in various ligands' structure which are aimed at the same target.

Table 4 Statistical parameters of CoMFA and CoMSIA models for the same training set based on docking alignment

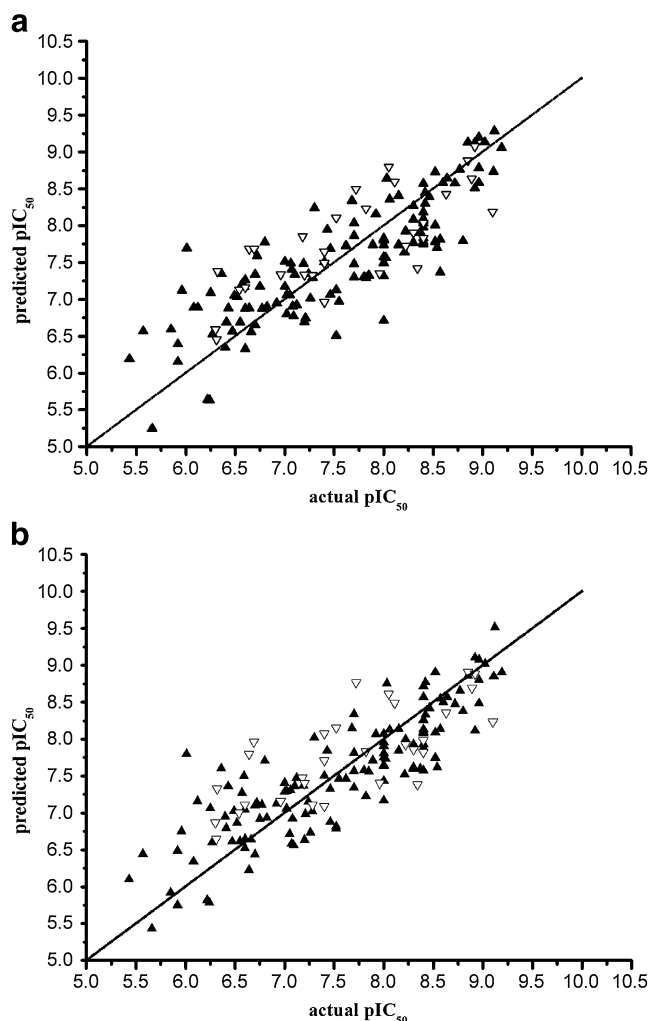|	ONC	PRESS	q^2	r^2	SE	F	Field contribution				
							steric	electrostatic	hydrophobic	donor	acceptor
CoMFA	2	0.664	0.507	0.695	0.526	139.885	0.470	0.530			
CoMSIA	3	0.697	0.463	0.734	0.493	112.037	0.217	0.225	0.220	0.106	0.233

Fig. 5 Correlation between the actual and predicted activities of 3D QSAR models based on docking alignment for the training set and test set as referred above. (a CoMFA model; b CoMSIA model. ▲: compounds of the training set; ▽: compounds of the test set)

The value of r (in Table 5) of QSAR models both align database and flexible docking alignment based on the same test set is high; and therefore predictabilities of QSAR models are good. The QSAR model based on flexible docking alignment is more similar with the real situation.

CoMFA and CoMSIA contour maps are displayed as STDEV*COEFF plots with compound 32, 39, 55 and 60, which have reference structures. The CoMFA electrostatic contour map is shown in Fig. 6a. The blue contour near 6′-position of the aniline ring (see the molecular in Table 1 for the atom numbering, same as below) is observed indicating the electropositive potential of the substituents should enhance the activity. This conclusion contradicted the previous built QSAR model in R. Thaimattam's work [21] which had strongly suggested electronegative substituent at

the 2′-position might enhance the activity. This contradiction would be discussed in detail in the following part. According to the molecular 82, 99, 100 and 101 in the dataset (see Table 1), the four molecular has the same structure except in the 6′- position , while the 6′ substituted atom is Cl, F, Br or I respectively, the activity (IC_{50}) increases ($7.28 < 7.52 < 8.00 < 8.21$) by the decreasing electro-negativity of the halogen atoms(F>Cl>Br>I). In addition, molecular 110, 113, 114 which also posses the same structure except varying the 6′- position——— Cl, F, Br, due to the decreasing electro-negativity: F>Cl>Br, the value of IC_{50} increases ($7.18 < 8.37 < 8.52$). This phenomenon gives us further proof that we can improve the IC_{50} by means of decreasing the electro-negativity of halogen atoms in 6′- position. A large red contour near CN group favored electronegative group at the 3-position.

The CoMFA steric contour plots are shown in Fig. 6b. The yellow contours near the aniline ring suggest any bulky substituent at this site is likely to decrease the activity (i.e., 70-74). The green polyhedrons observed near the 7-position suggested that bulky group substitution with moderate length might be preferred at this site (i.e., 145, 147).

The CoMSIA electrostatic and steric contour plots shown in Fig. 6c and d are consistent to that of CoMFA. The CoMSIA hydrophobic contour plot is shown in Fig. 6e. The yellow polyhedrons at the 4-position indicate a hydrophobic group substitution is favored at this site. In addition, a white polyhedron is also found at 7-position, that indicates any hydrophilic group substitution would be preferred at this site.

The CoMSIA hydrogen-bond donor and acceptor contour plot is presented in Fig. 6f. The magenta contour near the group substitution at 7-position indicates hydrogen-bond acceptor group might be favored.

The fields may hardly explain the interactions between the inhibitor and the enzyme. However, we could acquire enough information for modification of the reported inhibitors. The following statements are the results of our

Table 5 Comparison of the methods for the predictabilities of QSAR models based on both align database and docking alignment same test set (30 compounds)

	QSAR model based on align database		QSAR model based on docking alignment	
	r^2	r	r^2	r
CoMFA	0.60029066	0.77478427	0.52475968	0.72440298
CoMSIA	0.65528017	0.80949377	0.48410396	0.6957758

r – correlation coefficient
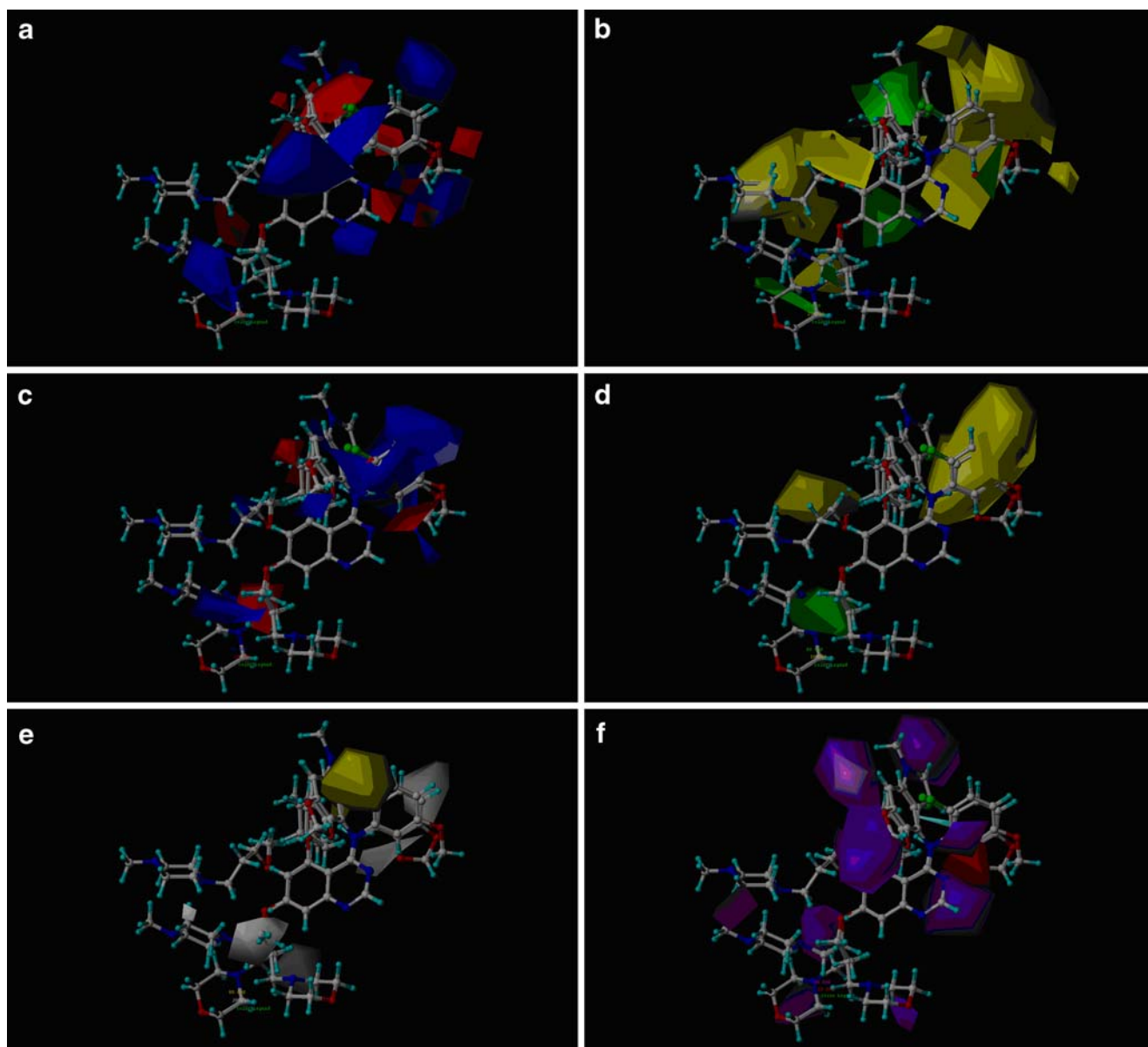
r^2 – square of correlation coefficient

Fig. 6 CoMFA (**a** and **b**) and CoMSIA (**c**, **d**, **e** and **f**) contour maps. Positive-charge-favored areas (contribution level of 80%) in blue. Positive-charge-unfavored areas (contribution level of 20%) in red. Sterically favored areas (contribution level of 80%) in green. Sterically unfavored areas (contribution level of 20%) in yellow. Acceptor-favored areas (contribution level of 90%) in magenta. Acceptor-unfavored areas (contribution level of 10%) in red. Donor-favored areas (contribution level of 90%) in cyan. Donor-unfavored areas (contribution level of 10%) in purple. Hydrophobic favored areas (contribution level of 80%) in yellow. Hydrophobic unfavored areas (contribution level of 20%) in white. Compound 32, 39, 55, and 60 were chosen as the reference molecules in the maps

docking studies, which are complements of 3D-QSAR studies for drug design.

As the QSAR models were derived by docking molecular structure into the binding site, it's interesting if one describes the contour maps in relation to the enzyme site structure. Superimposition of the docked conformation of compound 32 over the c-Src kinase binding site was depicted in Fig. 7.

Figure 7a depicts how bulky residues in the binding site can be correlated with the CoMFA steric contour maps. The yellow contour maps could be seen in most of the space around the molecule except one position outside of the molecule, where a green contour exists. These contours convey that Thr338, Tyr340, Ala403, and Asp404 in the binding site limit any bulky inhibitor.
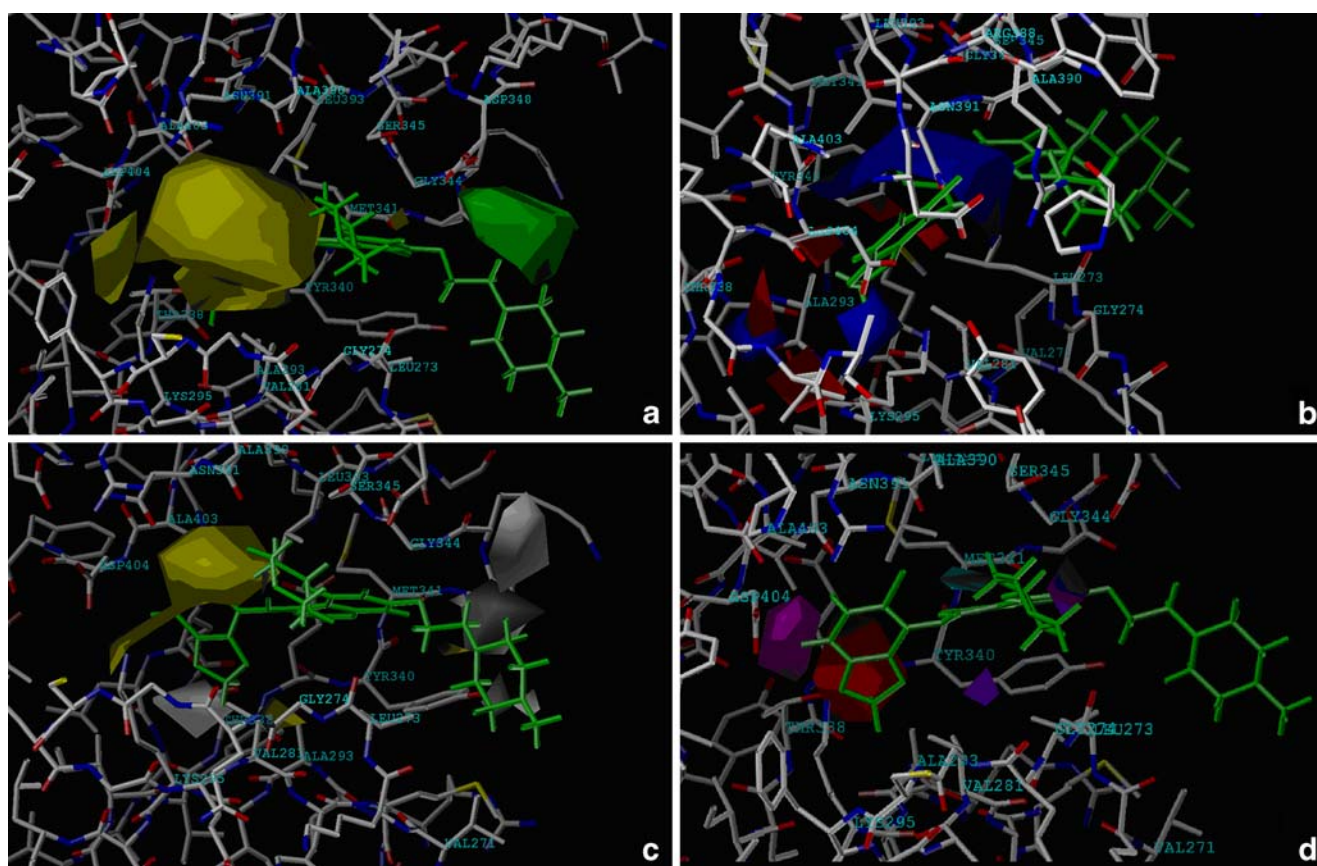
Fig. 7 The contour maps QSAR models with the docked inhibitor 32 and the amino acids involved in the binding site. **a** CoMFA steric field contour maps (green: favored; yellow, disfavored); **b** CoMFA electrostatic field contour maps (red: disfavored areas of positive potential, blue: favored areas of positive potential); **c** CoMSIA hydrophobic field contour maps (yellow: favored, white regions disfavored). **d** CoMSIA acceptor field contour maps (magenta: favored, red: disfavored)

In Fig. 7b, the CoMFA electrostatic contour maps, the blue regions near 6′-position of the aniline ring indicate that the positive groups may enhance the activity by interacting with residues Asp404— residues of acidic amino acid contain negative charge.

Figure 7c and d were obtained from CoMSIA. The presence of the hydrophobic residues such as Leu393 and Ala403 in the vicinity of the yellow regions near 4-position is clearly visible (Fig. 7c), which indicated the requirement of improvement of the hydrophobic interaction. Figure 7d shows the hydrogen bond acceptor field contour maps. Several magenta regions near 4′-position of the aniline ring proposed that hydrogen bond acceptors (for example, O, N, halogen and so on) in an inhibitor close to the hydroxyl group of residues Asp404 could increase the bind activity.

Conclusions

Robust CoMFA and CoMSIA models were obtained with a high predictive performance for the c-Src inhibitor training set and test set. Analysis of model parameters and contour maps revealed the factor that influenced the activity of those compounds for c-Src polymerase. The binding conformations of 156 derivatives into the c-Src allosteric binding pocket were predicted by the program DOCK6.0. Available 3D-QSAR models were also obtained based on the flexible docking alignment. The 4-position suggests that moderate size and hydrophobic group substitution is favored, which fits to the hydrophobic region that consist of hydrophobic residues in the active pocket. Similarly, bulky group substitution with moderate length might be preferred at 7-position, but hydrophilic group substitution is favored at this site. Small size and weak electronegative substituent in 6′-position of the aniline ring might enhance the activity. The 4′-position of the aniline ring shows that hydrogen bond acceptors in an inhibitor close to the hydroxyl group of residues Asp404 may increase the bind activity. The information obtained from those QSAR models may provide the tools for predicting the affinity modifying of related compounds and for guiding future structural synthesizing new potent c-Src inhibitors.

References

1. Thomas SM, Brugge JS (1997) Celluar functions regulated by src family kinases. Annu Rev Cell Dev Biol 13:513–609

2. Russello SV, Shore SK (2004) SRC in human carcinogenesis. Front Biosci 9:139–144

3. Tsygankov AY, Shore SK (2004) Src: regulation, role in human carcinogenesis and pharmacological inhibitors. Curr Pharm Des 10:1745–1756

4. Summy JM, Gallick GE (2003) Src family kinases in tumor progression and metastasis. Cancer Metastasis Rev 22:337–358

5. Aligayer H, Boyd DD, Heiss MM, Abdalla EK, Curley SA, Gallick GE (2002) Activation of Src kinase in primary colorectal carcinoma: an indicator of poor clinical prognosis. Cancer 94:344–351

6. Boyer B, Bourgeois Y, Poupon MF (2002) Src kinase contributes to the metastatic spread of carcinoma cells. Oncogene 21:2347–2356

7. Irby RB, Yeatman TJ (2002) Increased Src activity disrupts cadherin/ catenin-mediated homotypic adhesion in human colon cancer and transformed rodent cells. Cancer Res 62:2669–2674

8. Avizienyte E, Wyke AW, Jones RJ, McLean GW, Westhoff MA, Brunton VG, Frame MC (2002) Src-induced de-regulation of E-cadherin in colon cancer cells requires integrin signalling. Nat Cell Biol 4:632–638

9. Nam JS, Ino Y, Sakamoto M, Hirohashi S (2002) Src family kinase inhibitor PP2 restores the E-cadherin/catenin cell adhesion system in human cancer cells and reduces cancer metastasis. Clin Cancer Res 8:2430–2436

10. Rahimi N, Hung W, Tremblay E, Saulnier R, Elliott B (1998) c-Src kinase activity is required for hepatocyte growth factor-induced motility and anchorage-independent growth of mammary carcinoma cells. J Biol Chem 273:33714–33721

11. Jones RJ, Avizienyte E, Wyke AW, Owens DW, Brunton VB, Frame MC (2002) Elevated c-Src is linked to altered cell-matrix adhesion rather than proliferation in KM12C human colorectal cancer cells. Br J Cancer 87:1128–1135

12. Brunton VG, Avizienyte E, Fincham VJ, Serrels B, Metcalf CA, Sawyer TK (2005) Frame identification of Src-specific phosphorylation site on focal adhesion kinase: dissection of the role of Src SH2 and catalytic functions and their consequences for tumor cell behavior. Cancer Res 65:1335–1342

13. Duxbury MS, Ito H, Zinner MJ, Ashley SW, Whang EE (2004) Inhibition of SRC tyrosine kinase impairs inherent and acquired gemcitabine resistance in human pancreatic adenocarcinoma cells. Clin Cancer Res 10:2307–2318

14. Trevino JG, Summy JM, Lesslie DP, Parikh NU, Hong DS, Lee FY, Donato NJ, Abbruzzese JL, Baker CH, Gallick GE (2006) Inhibition of Src expression and activity inhibits tumor progression and metastasis of human pancreatic adenocarcinoma cells in an orthotopic nude mouse model. AJP 168:962–972

15. Levitzk A, Gazit A (1995) Tyrosine kinase inhibition: an approach to drug development. Science 267:1782–1788

16. Maly DJ, Choong IC, Ellman JA (2000) Combinatorial target-guided ligand assembly identification of potent subtype-selective c-Src inhibitors. Proc Natl Acad Sci 97:2419–2424

17. Dow RL, Bechle BM, Chou TT, Goddard C, Larson ER (1995) Bioorg Med Chem Lett 5:1007–1010

18. Hanke JH, Gardner JP, Dow RL, Changelian PS, Brissette WH, Weringer EJ, Pollok BA, Connelly PA (1996) Discovery of a Novel, Potent and Src Family-selective Tyrosine Kinase Inhibitor. J Biol Chem 271:695–701

19. Myers MR, Setzer NN, Spada AP, Zulli AL, YJ HC, Zilberstein A, Johnson SE, Hook LE, Jacoski MV (1997) The preparation and sar of 4-(anilino), 4-(phenoxy), and 4-(thiophenoxy)-quinazolines: Inhibitors of $p56l^{ck}$ and EGF-R tyrosine kinase activity. Bioorg Med Chem Lett 7:417–420

20. Thompson AM, Rewcastle GW, Boushelle SL, Hartl BG, Kraker AJ, Lu GH, Batley BL, Panek RL, DH SH, Denny WA (2000) Synthesis and Structure-Activity Relationships of 7-Substituted 3-(2, 6-Dichlorophenyl)-1, 6-naphthyridin-2(1H)-ones as Selective Inhibitors of pp 60c-Src. J Med Chem 43:3134–3360

21. Thaimattam R, Daga PR, Banerjee R, Iqbal J (2005) 3D-QSAR studies on c-Src kinase inhibitors and docking analyses of a potent dual kinase inhibitor of c-Src and c-Abl kinases. Bioorg Med Chem 13:4704–4712

22. Cramer RD, Patterson DE, Bunce JD (1988) Comparative molecular field analysis (CoMFA). 1. Effect of shape on binding of steroids to carrier proteins. J Am Chem Soc 110:5959–5967

23. Klebe G, Abraham U, Mietzner T (1994) Molecular similarity indices in a Comparative Analysis (CoMSIA) of drug molecules to correlate and predict their biological activity. J Med Chem 37:4130–4146

24. Cao HY, Zhang HB, Zheng XF, Gao DB (2007) 3D QSAR studies on a series of potent and high selective inhibitors for three kinases of RTK family. J Mol Graphics 26:236–245

25. Zhou ZG, Madura JD (2004) CoMFA 3D-QSAR analysis of HIV-1 RT nonnucleoside inhibitors, TIBO derivatives based on docking conformation and alignment. J Chem Inf Comput Sci 44:2167–2178

26. Cui M, Huang X, Luo X, Briggs JM, Ji R, Chen K, Shen J, Jiang H (2002) Molecular docking and 3D-QSAR studies on gag peptide analogue inhibitors interacting with human cyclophilin A. J Med Chem 45:5249–5259

27. Buolamwini JK, Assefa H (2002) CoMFA and CoMSIA 3D QSAR and docking studies on conformationally-restrained cinnamoyl HIV-1 integrase inhibitors: exploration of a binding mode at the active site. J Med Chem 45:841–852

28. Hennequin LF, Allen J, Breed J, Curwen J, Fennell M, Green TP, Lambert-van der Brempt C, Morgentin R, Norman RA, Olivier A, Otterbein L, Ple PA, Warin N, Costello G (2006) N-(5-Chloro-1, 3-benzodioxol-4-yl)-7-[2-(4-methylpiperazin-1-yl)ethoxy]-5-(tetrahydro-2H-pyran-4-yloxy)quinazolin-4-amine, a novel, highly selective, orally available, dual-specific c-Src/Abl kinase inhibitor. J Med Chem 49:6465–6488

29. Ple PA, Green TP, Hennequin LF, Curwen J, Fennell M, Allen J, Lambert-van der Brempt C, Costello G (2004) Discovery of a new class of anilinoquinazoline inhibitors with high affinity and specificity for the tyrosine kinase domain of c-Src. J Med Chem 47:871–887

30. Kuntz ID (1992) Science 257:1078–82

31. Ewing TJA, Makino S, Skillman AG, Kuntz ID (2001) J Comput-Aid Mol Des 15:411–428

32. DesJarlais RL, Sheridan RP, Seibel GL, Dixon JS, Kuntz ID, Venkataraghavan R (1988) J Med Chem 31:722–729